GeoHazards

Article

Tectonic Control of Aseismic Creep and Potential for Induced Seismicity Along the West Valley Fault in Southeastern Metro Manila, Philippines

Rolly E. Rimando [1,2,*] and Peter L. K. Knuepfer [2]

[1] Department of Science and Technology-Philippine Institute of Volcanology and Seismology (DOST-PHIVOLCS), Diliman, Quezon City 1101, Philippines
[2] Department of Earth Sciences, State University of New York, P.O. Box 6000, Binghamton, NY 13902-6000, USA; knuepfr@binghamton.edu
* Correspondence: rolly.rimando@phivolcs.dost.gov.ph; Tel.: +63-2-9207058

Abstract: Vertical creep along 15 ground ruptures within a 15 km long and 1.5 km wide zone has been occurring along the southeastern part of Metro Manila. Though the unusually high rates of vertical slip point to excessive groundwater withdrawal as the trigger, the evidence presented herein indicates that these may not be simple irregular subsidence fissures. Tectonic control of creep along these traces is suggested by the following: the occurrence of some of these ground ruptures along pre-existing scarps that coincide with topographic and lithologic boundaries, the left-stepping en echelon pattern of surface rupturing, and the distribution of the creeping zone within the dilational gap of the dextral strike-slip West Valley Fault (WVF). Furthermore, interpretation of an exposure across one of the creeping faults indicates reactivation by creep of a pre-existing tectonic fault zone. The paleoseismic evidence also suggests that the pre-creep slips are coseismic and dominantly strike-slip. Recognizing the occurrence of coseismic slip preceding aseismic creep is a primary consideration in assessing the potential of the WVF's creeping segment and its adjacent segments in generating earthquakes. Tighter groundwater extraction regulations may be necessary to avoid exacerbating the effects of vertical ground deformation and the occurrence of induced seismicity.

Keywords: aseismic creep; tectonic control; dilational jog; groundwater withdrawal; induced seismicity

Citation: Rimando, R.E.; Knuepfer, P.L.K. Tectonic Control of Aseismic Creep and Potential for Induced Seismicity Along the West Valley Fault in Southeastern Metro Manila, Philippines. *GeoHazards* **2024**, *5*, 1172–1189. https://doi.org/10.3390/geohazards5040055

Academic Editor: Riccardo Caputo

Received: 16 September 2024
Revised: 11 October 2024
Accepted: 22 October 2024
Published: 30 October 2024

1. Introduction

Vertical aseismic creep has been occurring along one of the segments (segment II) of the dextral strike-slip West Valley Fault (WVF) or West Marikina Valley Fault (WMVF), a large portion of which also straddles the eastern part of Metro Manila (Figure 1). The WVF and the East Valley Fault (EVF) are the two major segments of the right-lateral strike-slip Valley Fault System (VFS) or Marikina Valley Fault System (MVFS; Figure 1). The VFS is a relatively minor active fault to the west of the Philippine Fault Zone (PFZ; Figure 1), but its proximity to Metro Manila and other urban centers motivated the mapping of the active traces and the assessment of its seismic potential and hazards [1–4].

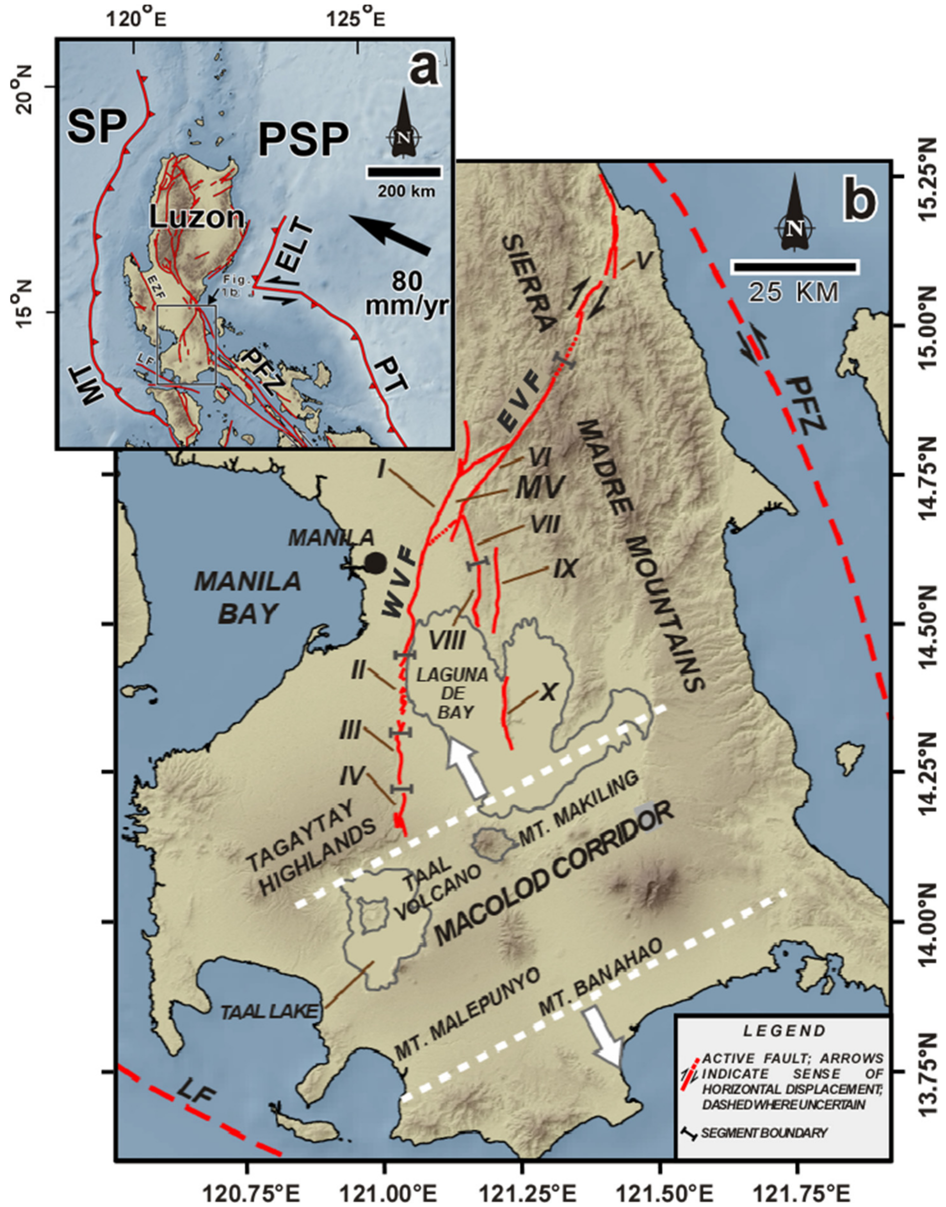

Figure 1. The creeping zone corresponds to a segment (Sucat–Biñan or segment II [3]) of the Valley Fault System (VFS) or Marikina Valley Fault System (MVFS) on the southeastern part of Metro Manila. The VFS belongs to a system of faults and subduction zones that accommodates part of the deformation in central Luzon due to the northwestward drift of the Philippine Sea Plate (PSP) towards the Sunda Plate (SP). (**a**) The VFS region is bounded by the Philippine fault zone (PFZ) on the east, the East Zambales Fault (EZF) on the west, and the Lubang Fault (LF) on the south. Also shown are the East Luzon Trough (ELT) and the Philippine Trench (PT) to the east and the Manila Trench to the west. Direction and rate of PSP motion after Seno et al. [5]. The active faults are from the Philippine Institute of Volcanology and Seismology [6], Rimando [2], Rimando and Knuepfer [3], and references therein. (**b**) The VFS extends for 135 km from the Sierra Madre to the eastern part of the Tagaytay Ridge. White dashed lines indicate approximate boundaries of the zone of volcanoes (Macolod Corridor) to the south of the VFS. White solid arrows indicate direction of extension within the Macolod Corridor. The northern part of the Marikina Valley (MV) is a pull-apart basin formed within the gap between the two major segments of the VFS (the West Valley Fault, or WVF, and the East Valley Fault, or EVF). The minor structural/geometric segments of the VFS are indicated by Roman numerals I to X. The creeping segment corresponds to segment II. Segmentation after Rimando [2] and Rimando and Knuepfer [3].

The identification of neotectonic landforms and offset morphotectonic and drainage features has greatly facilitated the mapping and identification of the VFS segments [2,3]. The lack of these features within the creeping portion of the WVF, however, posed a challenge in mapping the continuity of the WVF between segments I and III [2,3]. Aseismic creep was first recognized in 1994 along the 1.5 km wide and 15 km long zone between the segments [2–4]. Active fault mapping, which started in the 1990s before the occurrence of creep, was based mainly on the recognition of older scarps, which were assumed to be of tectonic origin [2,3], and along which most of the fresh vertical creep scarps occur (Figure 2a). It was suggested that the creeping ruptures are nontectonic subsidence "fissures" caused by excessive groundwater extraction [7] and that fissuring is more widespread in Metro Manila and surrounding areas due to the effects of subsidence [7–9]. Mainly due to the high rates of creep in the 1990s, there is unanimity about excessive groundwater extraction as the trigger of creep [2,4,7]. This study, however, maintains that the ground ruptures of the creeping zone are not irregular fissures. These are aseismic surface faults occurring along pre-existing active tectonic features associated with the WVF. Apart from the distribution of creep ruptures with respect to pre-existing scarps, we include the rupture pattern and the overall structural and kinematic context of fault creep in our analysis. Paleoseismic mapping, which had been used as a tool to verify multiple paleoseimic activity in the northernmost part of the WVF [1] along the segment north of the creeping zone, was employed to ascertain pre-creep tectonic activity from a fault exposure across one of the creeping segments.

The damage that vertical creep has been causing since the early 1990s provided primary impetus for this work. The ground rupture associated with creep has been causing damage to the ground, roads, and residential and commercial buildings (Figure 2b–h). Some roads and highways have become hazardous to motorists in several places due to the mainly vertical rupturing at rates as high as 20 cm/yr in the 1990s (Figure 3) [2,4]. The slip rates along the WVF's creeping segment are much higher compared with the known slip rates along active faults undergoing tectonic creep, which have led most studies to suggest that creep was triggered by excessive groundwater withdrawal. The aseismic portion of the San Andreas fault's creeping segment, the central segment, slips at a maximum rate of 35 mm/yr [10]. The short- to long-term lateral creep rate for the Hayward and Calaveras faults in California ranges from a few millimeters to 1.7 cm/yr [11–14]. Other examples of fault creep around the world that occur along strike-slip faults include the central segment of the Longitudinal Valley fault in Taiwan (1.0–2.0 cm/yr) [15] and the North Anatolian fault in Turkey (2.0 cm/yr) [16]. Rimando et al. [4] verified the spatial and temporal correlation between displacement/slip rate and groundwater extraction and confirmed the role of groundwater extraction in triggering and controlling fault creep. Although creep has substantially slowed down in recent years in the northern part of the creeping segment, displacement monitoring shows that slip rates remain relatively high in its southern part [4]. The slowing down in slip rates in the northern part of the creeping zone and the sustained high rates of slip in the southern part are attributed to the regional differences in groundwater extraction controls [4].

This paper documents and discusses the nature and control of the first known occurrence of anthropogenic surface-rupturing fault creep in the Philippines. Here, we characterize the unique characteristics of fault creep in the study area from results of surface mapping of the creeping traces. More specifically, we examine whether these fault traces represent irregular "subsidence" surface fissures or creep ground ruptures that follow a more ordered pattern. Whether the occurrence of fault creep is controlled by prior tectonic faulting will be explored through paleoseismic investigation of a stream exposure across one of the creeping traces. This work is an opportunity to examine the nature of fault creep and its relation to tectonic slip, a process that has not been investigated in the Philippines and only in part elsewhere. The results of this work also have implications for seismic hazard assessment involving the VFS.

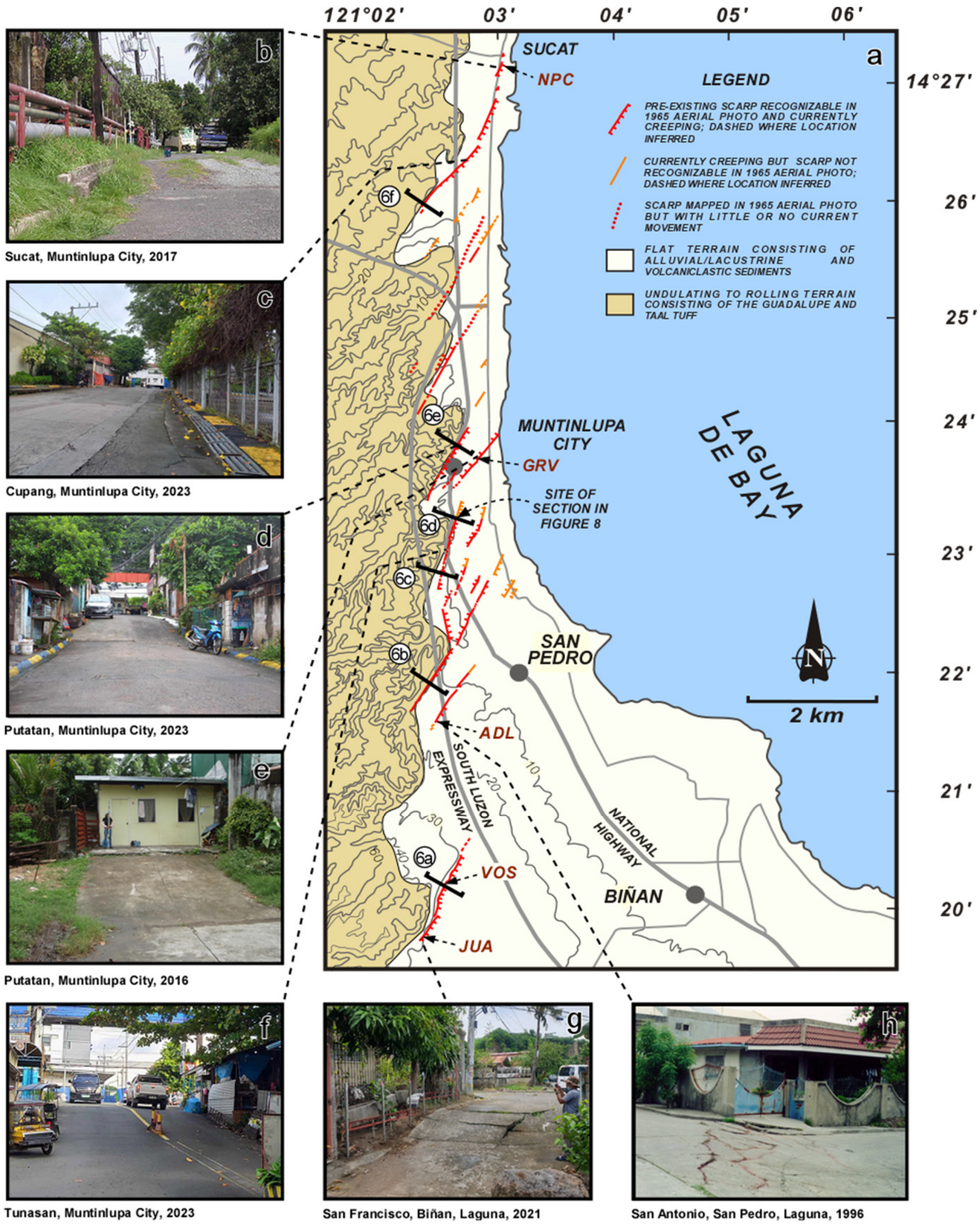

Figure 2. (**a**) The WVF creeping segment (segment II in Figure 1). The creeping zone consists of lithologic units derived from nearby volcanic centers. Most of the creeping faults occur along scarps identified in the 1965 aerial photos and in topographic maps based on older aerial photos. (**b**–**h**) Photos of vertical displacement and damages to ground and man-made structures along creep scarps. Locations and dates when photos were taken are indicated under each photo. For variation in displacement and slip/displacement rates, refer to Rimando et al. [4]. The encircled 6a to 6f and the symbol refer to the locations of scarp profiles used for height estimation. NPC, GRV, ADL, VOS, and JUA refer to deformation survey sites where displacements have been regularly measured (2–3 times/yr) since 1999. Slip rates derived from displacement measurement at these sites are in Figure 3. Source of *geology*: Bureau of Mines and Geosciences [17].

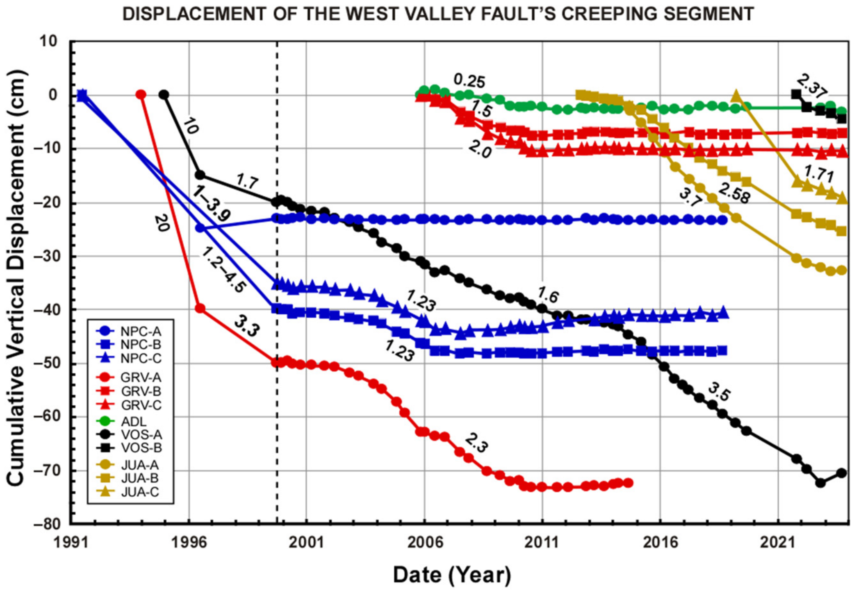

Figure 3. Plot of cumulative vertical displacement estimates from various sites within the creeping segment since the 1990s. The numbers are slip rates in cm/y. Displacements in the 1990s (left side of dashed vertical line) were measured using a hand level and a graduated telescoping rod. The 1999–2019 displacement data used are from Rimando et al. [4] and references therein. A more precise method using an electronic digital level, a bar-code leveling staff, and several fixed benchmarks was employed to generate the 1999–2019 displacement data by the joint Philippine Institute of Volcanology and Seismology–Tokyo Institute of Technology (PHIVOLCS-TIT) team. The 2019–2023 data were generated using the same method.

2. Materials and Methods

Detailed mapping of the creeping fault traces was first carried out in 1994, when creep was first observed. Field observation of the damage to man-made structures caused by ground rupturing was also instrumental in the mapping of the individual segments. Topographic maps, geologic maps, and aerial photos were analyzed to determine the distribution of creeping faults, establish the spatial association of creep occurrence with respect to topographic and lithologic boundaries, identify pre-creep scarps, and recognize any geometric pattern exhibited by the creeping segments. Post-World War II topographic maps and aerial photos were particularly useful in mapping and identifying pre-creep scarps of possible tectonic origin. Leveling surveys and the use of Google Earth were useful in recognizing and generating profiles for the purpose of measuring heights of active and pre-creep scarps. Comparisons of the active creep scarp heights with pre-scarp heights are critical in determining possible pre-creep tectonic activity.

The verification of the nature and type of prior tectonic activity along a pre-existing scarp was carried out through logging of an exposure near the central part of the creeping zone where one of the creeping segments crosses the Magdaong River (location in Figure 2a). We mapped fault strands and stratigraphic and soil horizons in the exposure in order to distinguish between creep and coseismic slip and to determine the type of any tectonic faulting involved. Lines of structural and sedimentary evidence had been used to distinguish between aseismic and coseismic activity in exposures [14,18–23]. The amounts of vertical separation, changes in thickness of faulted stratigraphic units, and upward termination of fault strands are among the most useful distinguishing criteria [14,18,22]. The above criteria have also been used to recognize the type of faulting involved. Weldon et al. [22], for example, discussed how these types of evidence are considered in exposures of strike-slip faults. A number of other criteria, including fault zone structures, filling materials, nature and attitude of contact, and shear fabric, are also useful in identifying the dominant type of faulting involved [18,20,24–26]. No age-dating other than relative age-dating based on stratigraphy was conducted, as mapping of the trench exposure was intended only to provide evidence of the nature (tectonic or nontectonic) and type of any pre-creep faulting from bed displacements and thicknesses and fault strand patterns and terminations.

3. Results and Discussion

3.1. Topographic, Lithologic, and Structural Context of Creep

The recognition of morphotectonic features and displaced landforms and streams had been instrumental in mapping the active traces of the VFS [2,3]. As Figures 2 and 4 show, scarps are the dominant geomorphic features within the creeping zone, which lies between segments I and III. The occurrence of creep was first reported during the initial stages of neotectonic mapping of the WVF in the early 1990s. The recognition of fresh creep scarps occurring on old scarps within the creeping zone, which were assumed to be of tectonic origin, greatly facilitated the mapping of the creeping zone (as segment II) and the continuity between segments I and III.

The first and longest ground rupture was mapped in the northernmost part of the study area (Figures 2a and 4) on 21 July 1994 [2]. The 2.6 km long ground rupture is similar to some portions of recent coseismic ground ruptures (e.g., ground rupture of the 1990 Luzon Earthquake) except that it is creeping and its displacement is dominantly vertical (Figures 2b–h and 4). Many of the NNE- to NE-striking creep scarps, especially on the western part of the creeping zone, follow larger scarps that coincide with the boundary between the regions of higher topographic relief and the low-lying areas beside the lake (Figure 2a). The creeping segments also coincide spatially, partly or wholly, with lithological contacts on the western part of the creep region (Figure 2a). As discussed in Section 3.2, these topographic boundaries consist of higher-order scarps, at or near the base of which the creeping fault traces have formed.

The creeping ground ruptures are not irregular fissures that occur randomly, as suggested by Ramos [7]. "Fissuring" had also been suggested to occur in Metro Manila and surrounding areas [7–9], but the creeping ground ruptures between segments I and III of the WVF are more appropriately classified under the surface fault type of aseismic ground failure [27,28] rather than the tensile type of failure [27,28]. It had been suggested that subsidence and fissuring due to groundwater withdrawal are regional in nature [7–9]. However, no creeping ruptures similar in amount of deformation, extent, and geometric pattern to those in the study area have been observed in the regions outside of the creeping zone. The fact that vertical deformation that is focused along discrete stepping faults occurs only near the western shore of the lake (Laguna de Bay) underscores the possible role of pre-existing structures in localizing creep phenomena.

The creep ruptures exhibit a left-stepping en echelon pattern along a north–south-striking zone (Figures 2a and 4). At the scale shown in Figures 2a and 4, the traces are essentially straight. Two pairs of creeping fault traces near the central part of the zone bound inner downthrown blocks that resemble pull-apart basins (and were also assumed to be pre-creep pull-apart basins). Although the dominantly vertical movement of the current creep is responsible for these features, pull-apart basins could also result from the movement of bounding strike-slip faults with large vertical components, which could have been the case before the onset of creep. It is unlikely that differential compaction alone had caused the development of the pull-apart basins. The occurrence of the en echelon scarps within the gap between the right-stepping WVF segments and the kinematic congruence of "pull-apart basins" with right-lateral strike-slip movement along segments I and III indicate that local tectonic stresses (Figure 4 inset) may have been involved in controlling the distribution and kinematics of the creeping ground ruptures. Though differential compaction of the materials across ground ruptures may have contributed significantly to the vertical displacement, groundwater withdrawal altered the balance of stresses acting on the fault plane, triggering the release of stored strain energy through movement along the ground ruptures. Groundwater withdrawal causes vertical load reduction and compaction of the aquifer [29,30]. The resulting reduction in normal stress contributes to fault failure, as implied by the Mohr–Coulomb failure criterion.

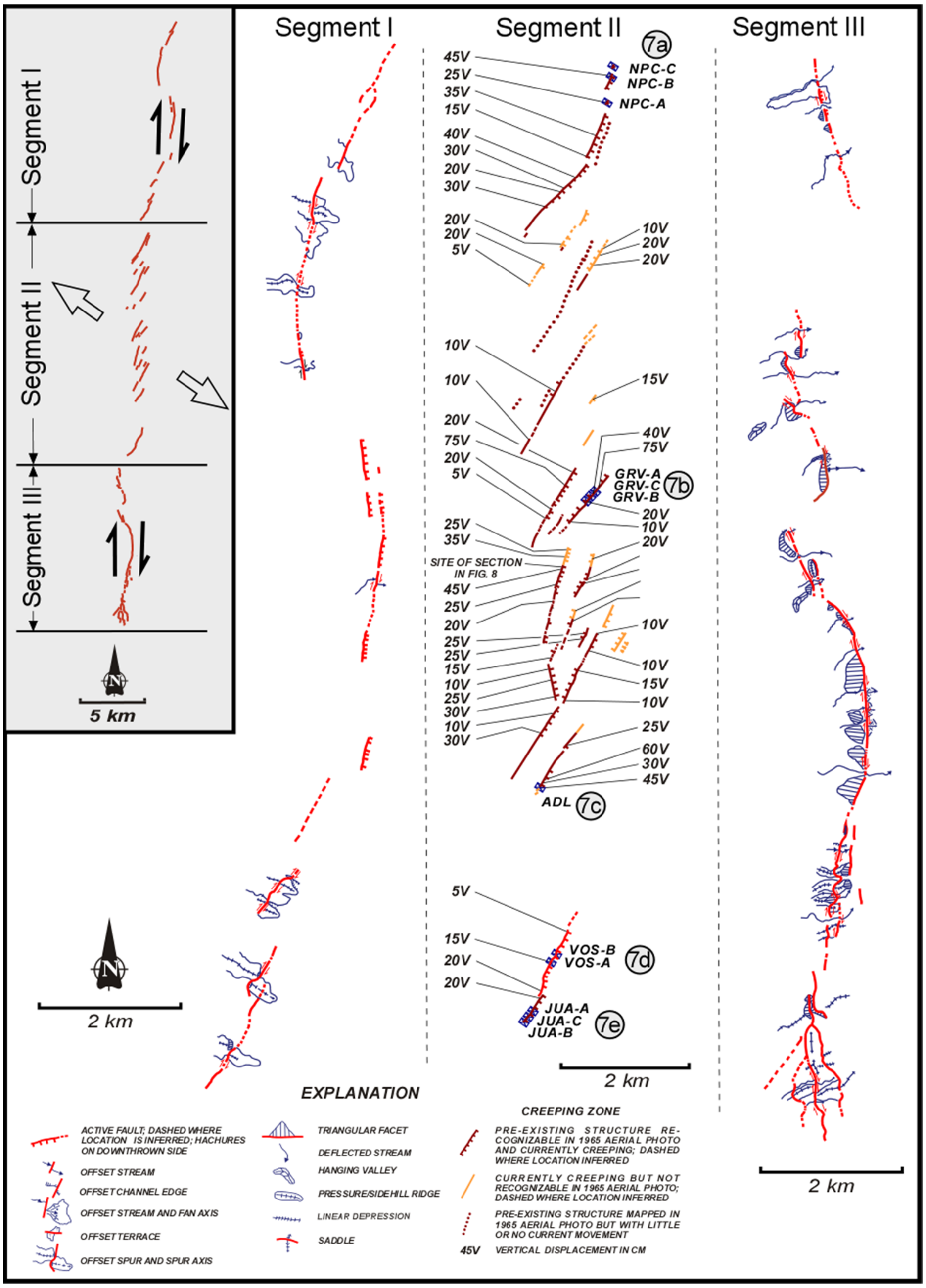

Figure 4. Segments I, II, and III of the WVF. The mapping of segments I and III and the rest of the VFS was based mainly on the recognition of offset features (e.g., streams and spurs) and landforms associated with active faults. The mapping of segment II was initially based on the recognition of old scarps and creep scarps, many of which followed the pre-existing scarps. The vertical displacements along the creeping segments were based on field measurements carried out mostly in 1996. The left portion of the plot in Figure 3 was constructed based on these measurements, while the right portion of the plot was based on the results of precise leveling that started in 1999 at sites labeled NPC, GRV, ADL, VOS, and JUA. The inset indicates the location of the segments and shows NW-SE extension (open arrows) within the dilation gap between segments I and III. The encircled 7a to e refer to the locations of scarp profiles derived from precise leveling data for height estimation. Site of paleoseismic section along segment II is also shown. Modified from Rimando [2] and Rimando and Knuepfer [3].

Structures with orientations similar to those of the scarps that the creeping ground ruptures followed are expected to have a large vertical component (as oblique strike-slip or normal faults) when activated by extension due to right-lateral strike-slip faulting along N-S master faults (Figure 4 inset). Largely because of this unique rupture and scarp pattern and occurrence within the gap area between the right-stepping segments (segments I and III in Figures 1, 2 and 4) of the WVF [2–4], the creeping zone has been considered a distinct segment of the WVF.

3.2. Creep Displacements and Pre-Creep Scarp Heights

The displacements, which are largely vertical, were measured along the fifteen ground ruptures during the 1994 to 1996 mapping period in the Muntinlupa–San Pedro–Biñan area (Figure 2a). The maximum vertical displacement measured was ~0.75 m in Muntinlupa City near the central part of the creeping zone. Minor amounts of apparent lateral component were observed where offset markers are oblique to the strike of the fault.

The differences between creep displacements and heights of pre-creep scarps seem substantial. This is exemplified by a creep scarp that is situated near the foot of an old scarp (Figure 5a). The creep scarp height is 0.7 m as measured by precise leveling in March 2024. The active creep scarp at Juana in Figure 5a belongs to the southernmost creeping segment (Figure 2a). The host pre-creep scarp is visible on the old topographic map (Figure 5b) and post-war aerial photos (Figure 5c). The host scarp is considered pre-creep since the 1:50,000-scale topographic map in Figure 5b was based on 1947–1952 aerial photos while the aerial photos in Figure 5c were taken in 1966. The large discrepancy in displacement is also exemplified by creep scarp displacement (Figure 5d) and pre-creep scarp height measurements at Villa Olympia Subdivision (VOS) along the southernmost creeping segment (Figure 2a). The displacements and heights across the scarp at VOS were derived from profiles generated through precise leveling surveys in 1999 and 2023 (Figure 5e). The difference in scarp heights between the two profiles in Figure 5e represents creep displacement between 1999 and 2023. The total amount of creep displacement at VOS since the 1990s is the sum of 1999–2023 creep displacement and the displacement measured in the 1990s (Figure 3). A height of 7 m is estimated for the larger scarp based on the 2023 VOS-A scarp profile in Figure 5b (drawn oblique to the scarp) and Figure 6a (drawn perpendicular to the scarp). It represents an increase of 0.5 m from a height of 6.48 m in 1999. If the displacement that had occurred (from the time creep is presumed to have started at VOS) until September 1999 (20 cm; see Figure 3) [4] is added to this, the contribution of creep to the 2023 scarp height is 70 cm. This is almost an order of magnitude smaller than the estimated total displacement (7 m).

The northernmost and southernmost creeping segments are on the west side of the zone, where the creep scarps strongly correlate with the topographic and lithologic contacts. The profiles drawn across other scarps on the west side of the zone (Figure 6) also indicate much larger heights compared with the displacements due to the ongoing creep (Figure 4; Figure 7). In addition to the VOS profile, sections across the other displacement monitoring sites (NPC, GRV, ADL, and JUA) were also drawn from precise leveling data (Figure 7). These represent the scarps due to the ongoing creep, as the displaced references (i.e., roads) were built at about the same time of creep initiation [2,4]. With the exception of NPC, all sites are still being surveyed periodically. There are no remarkable pre-creep scarps associated with the creep scarps on the eastern side of the creeping zone. The creep scarps at these sites occur in highly developed and built-up areas and where erosion and sedimentation are more likely to have prevented the preservation of pre-creep surface scarps. Nevertheless, creep-related scarp displacements at these sites (see GRV and ADL profiles in Figure 6b,c; see Figure 4 for site location) are also mostly no more than 1 m, which are almost an order of magnitude lower than the heights of pre-existing scarps at adjacent sites on the west part of the creeping zone (Figure 6). As Figure 3 also shows, the total creep displacements at the other displacement monitoring sites (see Figures 2 and 4 for location of monitoring sites) are mostly no more than 1 m. The total creep displacement at NPC-A, NPC-B, NPC-C, GRV-A, and VOS-A is the sum of displacement derived from precise leveling (right side of displacement plot) and the 1990s displacements (left side of displacement plot). The 1990s displacements in various parts of the creeping zone are shown in Figure 2.

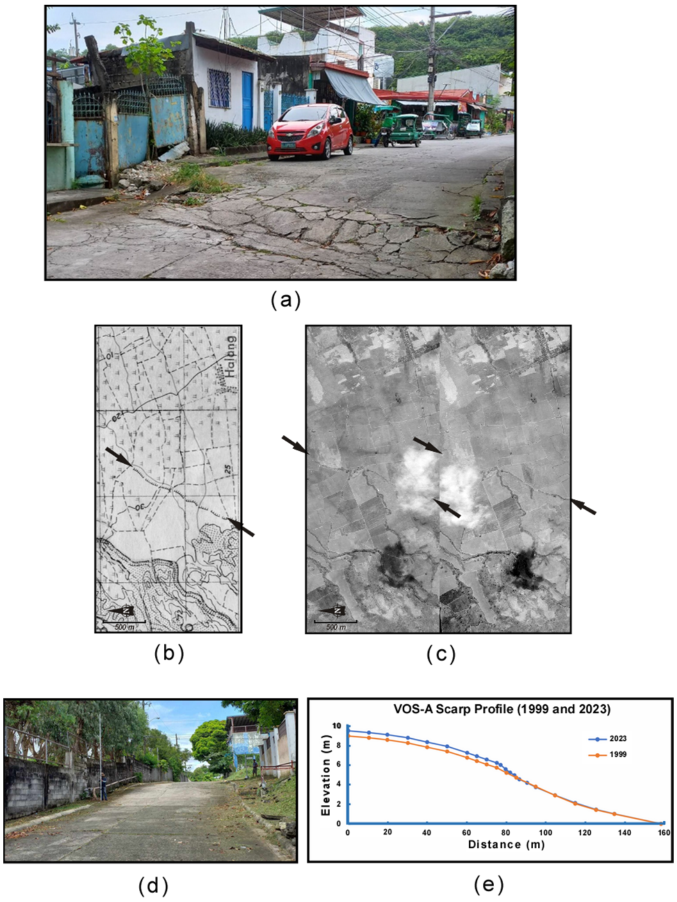

Figure 5. (**a**) Ground rupture along the southernmost segment of the creeping zone. Creep scarp occurs near the foot of an old scarp at Juana Subdivision, Biñan, Laguna. (**b**) Evidence of pre-creep scarp coinciding with the creeping zone's southernmost segment (see Figure 2). The scarp is indicated by hachures (location marked by arrows) on a 1:50,000-scale topographic map that was drawn based on 1947–1952 aerial photos. North points to the left side of the figure and is parallel to the gridline. Ground ruptures in (**a**) occur near the southernmost part of the segment. (**c**) Stereopair of the general area from 1966 aerial photos showing the same scarp in (**b**). (**d**) The active creep scarp at Villa Olympia Subdivision (VOS) (San Pedro, Laguna) along the southernmost creeping segment at VOS, which also occurs along the scarp in the topographic map in (**b**) and in the 1966 aerial photo (**c**). Photo taken in September, 2023. Part of the road across the scarp had been resurfaced. The creep scarp, which appears to be superimposed on a pre-existing scarp, was first noticed in 1996 when it was only ~0.15 m high, but it reached a height of 0.725 m by 2022. (**e**) Profiles of the larger scarp hosting the active scarp were based on the precise leveling surveys conducted in 1999 and 2023. Profiles were drawn along the road, which is oblique to the NE-trending scarp. The estimated total scarp heights were 6.48 m and ~7 m in 1999 and 2023, respectively. Figure 6a shows a profile taken along a line close to and perpendicular to the scarp in (**d**).

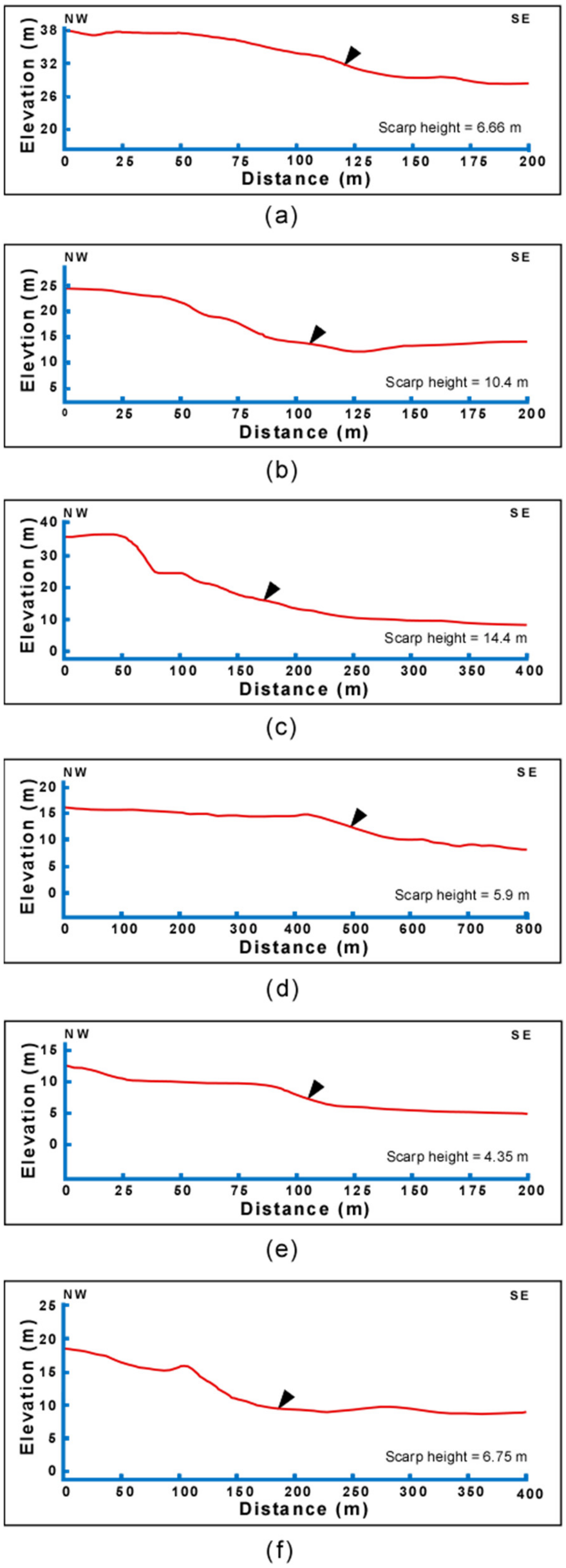

Figure 6. Profiles drawn perpendicular to the segments on the western part of the WVF's creeping zone (segment II). The arrows indicate the location of the scarps due to the current creep. The locations of the profiles (**a**–**f**) are indicated in Figure 2a. Scarp height estimates are indicated.

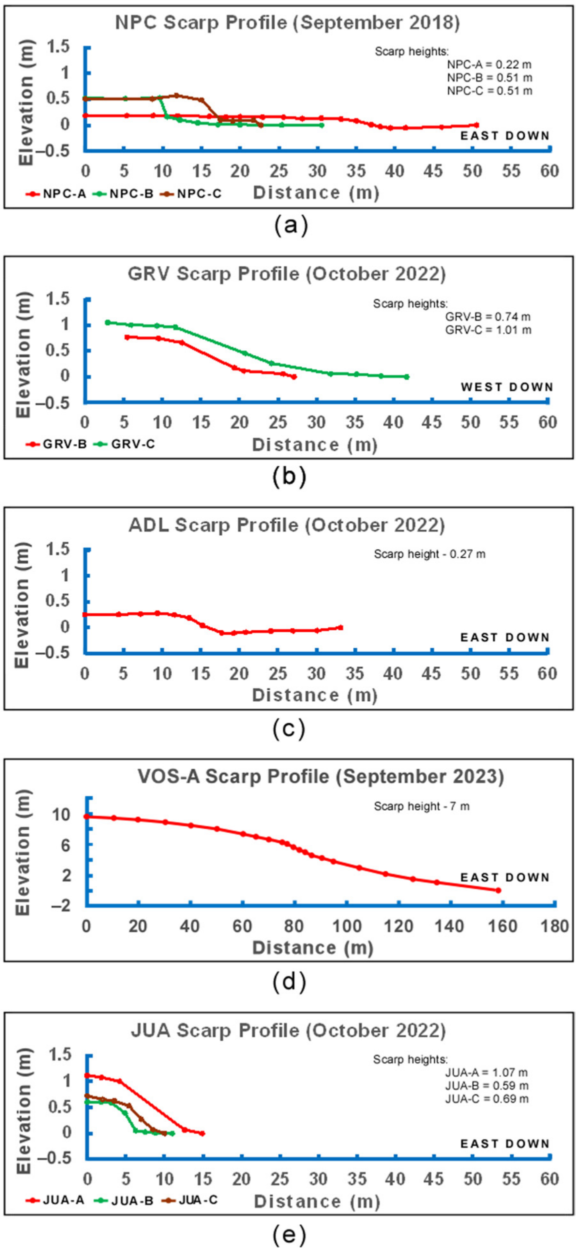

Figure 7. Profiles across selected creeping segments in 5 precise leveling sites. The locations of the profiles (**a**–**e**) are indicated in Figure 4. Scarp height estimates are shown for each profile.

The large differences between the heights of the pre-creep scarps and the displacements due to the current creep suggest possible multiple surface-rupturing events along the larger scarps. The fact that the region only saw the start of significant development in the 1980s and that there are no reports of earlier creep occurrences makes it unlikely that the higher scarps are products of earlier creeping events. Furthermore, the fact that the pre-creep features are also recognized in old topographic maps (based on 1947–1952 aerial photos) makes it more unlikely that these are products of the ongoing creep event.

3.3. Paleoseismic Mapping of Creeping Segment Exposure

As creep may occur along pre-existing scarps that are nontectonic in origin, paleoseismic mapping was employed to verify whether tectonic faulting preceded and played a role in localizing creep. The highly urbanized nature of the creeping zone poses tremendous challenges in identifying trenching sites. An exposure along a river cut by one of the creeping faults in Muntinlupa City (Figure 8a; location in Figures 2a and 4) provided an opportunity for mapping fault strands and offset sedimentary units without excavating.

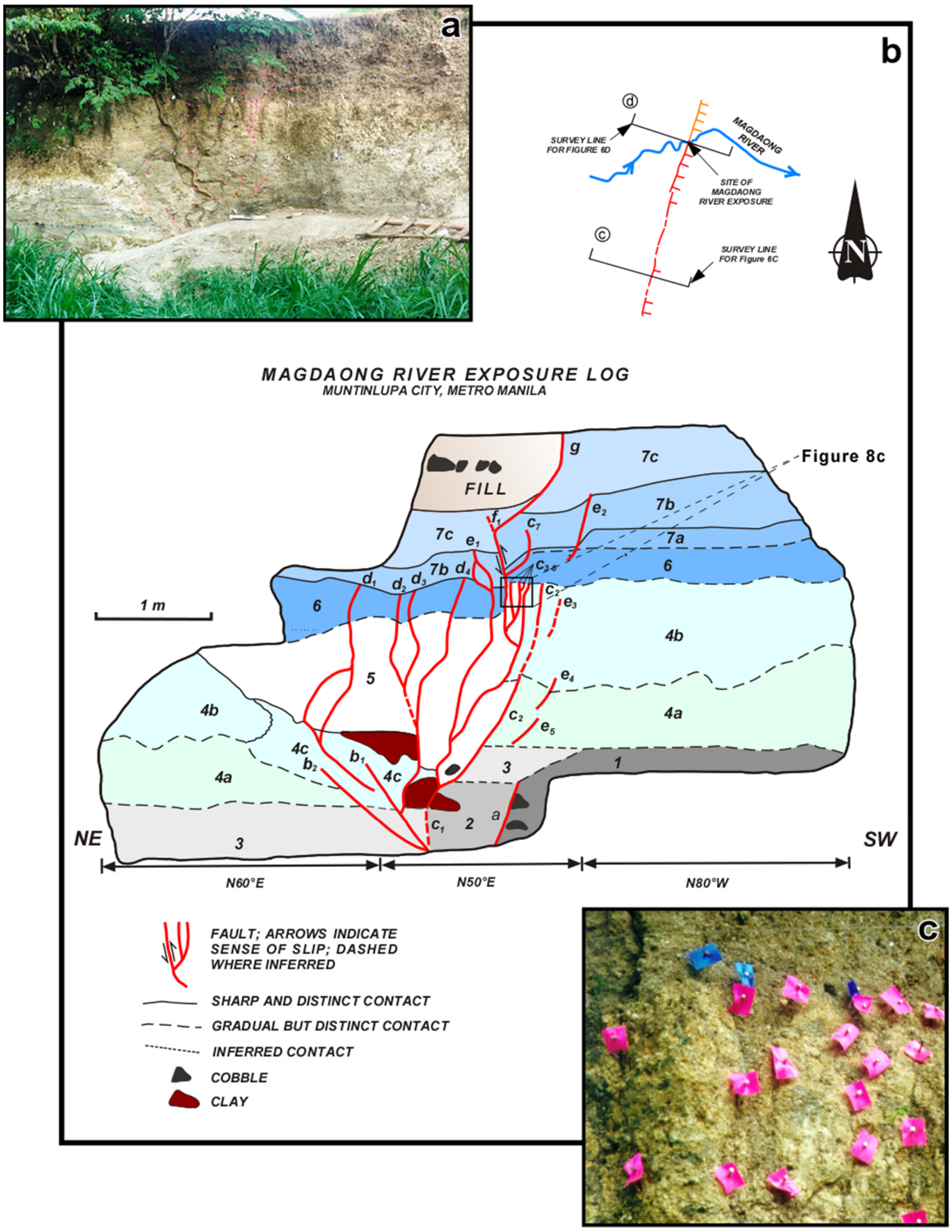

Figure 8. (**a**) Section of stream exposure across one of the creeping traces at Magdaong River, Muntinlupa City. Exposure shows prior surface-rupturing events, which were, most likely, generated by strike-slip faulting. (**b**) Simplified log of stream exposure across one of the creeping traces at Magdaong River, Muntinlupa City. The location of the site is indicated in Figures 2 and 4. Older strike-slip fault ruptures cut through buried sediments only, while modern creep has vertically displaced the present surface. Fault contact between units 2 and 3 at the bottom part of the section is indistinct, so this part of the log is quite interpretive. The section was originally logged at a 1:20 scale. Descriptions of stratigraphic units appear in Table 1. The numbered letters refer to fault strands. The upper right part of the figure also shows the location of scarp profiles c and d in Figure 6 and of the Magdaong River exposure. (**c**) The upward termination of fault strands c_3 to c_6 at the base of unit 6 represents one pre-creep event, interpreted as a sudden coseismic slip. Location of photo shown in (**b**).

Table 1. Description of stratigraphic units in the Magdaong River exposure.

Unit No.	Genesis	Matrix Texture	Texture		Clast Distribution	Lower Boundary	Stratification	Other Features
			% Pebbles	% Cobbles				
1	Fluvial/Colluvial	Silty Clay	0	0	Isolated	Not Exposed	Massive and as lenses	Clay as lenses and as cobble-sized or larger clay balls
2	Fluvial/Colluvial	Matrix-supported (sandy)	~80	0	Evenly distributed	Not Exposed	Massive	Sandy and pebbly with balls of clay and lenses of clay and sand
3	Stream Channel	Clayey sand	>50 in upper 10–15 cm	0	Upper: stratified, continuous Lower: evenly dispersed	Upthrown: clear, smooth to wavy Downthrown: not exposed	Upper: clear, interbedded Lower: Massive	Upper 10–15 cm cross stratified and with larger fragments of pebbles; lower is coarse sand
4a	Stream Channel	Matrix-supported (coarse sand matrix)	40–50	0	Semi-stratified, discontinuous	Wavy, clear to diffused	Weak to massive	-
4b	Weathered 4a	Silty clay	0	0	NA	Gradual, wavy	Massive	With dark mottles
4c	Weathered 4a	Silty clay loam	7%	0	Evenly dispersed	Gradual, wavy	Massive	Lighter than 4b; also with mottles
5	Stream Channel	Matrix-supported (sandy)	~80	0	Stratified, continuous	Very abrupt, smooth	Weak to distinct, interbedded	-
6	Stream Channel	Matrix-supported (silty clay loam)	0–85	0	Evenly dispersed	Gradual, clear to wavy	Weak to massive	With rounded pebbles, coarser than pebbles as unit 5
7a	Colluvium	Sandy clay loam	25–40	0	Evenly dispersed	Gradual, wavy	Weak to massive	-
7b	Weathered 7a	Sandy loam	7–15	0	Evenly dispersed	Gradual to abrupt, wavy	Massive	-
7c	Soil	Sandy loam	0	1	Isolated	Gradual to abrupt, wavy	Massive	-
Fill	Fill	Loamy sand	40–50	15–20	Evenly dispersed	Abrupt, clear to smooth	Massive	With glass and plastic fragments

A log of the exposure (Figure 8b) along the Magdaong River shows mostly fluvial deposits representing reworked primary volcanic deposits from the slopes of the Taal Caldera to the west of the creeping zone. These are interbedded with layers of colluvium and soil. The soil layers (units 4b and c and 7c; Figure 8b) appear to be weathered counterparts of underlying fluvial and colluvial strata. Detailed descriptions of the faulted units are in Table 1.

Our mapping of the exposure at Magdaong River (Figure 8) shows only one strand cutting the present surface, which represents the ground rupture of the ongoing creep. Most of the strands terminate at the top or bottom of units. One strand terminates at the base of unit 3. Multiple fault strands terminate at the base of units 6 and 7 (Figure 8b,c). One of the earliest events that can be inferred with a high degree of confidence from the Magdaong section (Figure 8b) is represented by the termination of fault strands c_2 to c_6 at the base of unit 6 (Figure 8c). Following the burial of the stream channel deposits (units 4 and 5; Figure 7b) by a younger stream channel unit (unit 6; Figure 8b), another faulting episode ruptured through unit 6. The coseismic nature of this event is evident from the termination of fault strands d_1 to d_4 at the base of unit 7b. Two fault strands (e_1 and e_2) cut unit 7b and terminate at the base of unit 7c. These strands represent the youngest coseismic event. Unit 7c is considered an in situ soil layer; therefore, fault strands e_1 and e_2 are not surface-rupturing faults. However, a reactivation of e_2 by the current creep is indicated by the sagging of the base of units 7b and 7c.

Since we are not dealing with a three-dimensional exposure, we have avoided the over-estimation of the number of events by interpreting only the termination of multiple fault strands at the same stratigraphic level. In exposures that are not three-dimensional, single strands terminating at various levels may or may not represent separate events [18,22]. Thus, the nature of the single strand (strand a) terminating at the base of unit 3 is uncertain. The sharp lithological contrast across the "strand" indicates that it could be a fault, a channel wall, or both.

No colluvial wedge was found associated with any of the stratigraphic offsets in the section. This suggests a creep mechanism rather than coseismic slip [14,20]. At least the latest event is known to be causing creep along the single strand propagating to the present surface. The other fault strands may have been caused by creep if we use colluvial wedges alone as a criterion. However, colluvial wedges in strike-slip fault zones are generally thin and poorly differentiated due to the small height of the fault scarp [22]. Thus, if offsets on these strands were principally lateral slip, colluvial wedges may not have formed.

The bed offsets at the Magdaong River exposure log (Figure 8b) caused by both the ongoing creep and pre-creep activity were measured, and the vertical separation of the stratigraphic units across fault strands is shown in Table 2. Notable displacements are those of the bottom of unit 6, unit 7, and the bottom of unit 4 along fault strand g. The amount of vertical offset of the bottom of unit 6 is ~0.35 m along fault strand g. Historic creep along fault strand g was primarily responsible for the bulk of this displacement. Part of the displacement is due to prior slip along d_4 (~0.06 m), f_1, and probably e_1. Unit 7 is displaced by almost the same amount (0.35 m), also principally by creep along fault strand g. This roughly corresponds to the amount of displacement of the surface at and near the site. The cumulative displacement of the bottom of unit 4 is ~0.6 m. The difference between the displacement due to creep and the displacement of the lower units is ~0.25 m. This is far greater than the ~0.06 m displacement of the bottom of unit 6 along d_4. Based on the increases in displacement with depth, the strands terminating at the bottom of units 6 and 7b are most likely coseismic in nature. The displacement is likely due to a vertical component of coseismic slip along fault strands c_1 to c_6, and quite possibly, apparent vertical movement due to lateral displacement of unit 4. The type of coseismic faulting most likely involves a large component of strike-slip motion based on the upward-splaying pattern of the faults in the Magdaong exposure [22]. Other useful observations for establishing strike-slip faulting from the Magdaong exposure include the changes in thickness of units 3 and units 6 to 7b across the fault zone (Figure 8b) and the relatively minor progressive change in vertical component with depth (compared with the change with depth for the other types of faulting) in the exposure.

Table 2. Displacement of stratigraphic units along fault strands.

Unit Offset	Displacing Fault Strand	Amount of Offset (m)
1 and 2	a	Bottom offset indistinct
3	c_2 and g	Bottom offset indistinct
4	c_2 and g	~0.60
4b	e_4	0.04
4b	c_2	0.06
6	g	~0.35
6	d_4	0.06
7	g	0.35
7b and 7c	e_2	0.18
7c	g	0.35

Like the southernmost segment and most of the westernmost creeping segments, the ground rupture at Magdaong occurs along the topographic boundary and lithologic contact (Figure 2a). A profile drawn perpendicularly across the exposure shows that the active creep scarp also occurs on a larger scarp (~5 m; profile D in Figure 6d), which is substantially higher than the scarp generated by the current creep activity. Profile C in Figure 6c, which was taken south of profile D along the segment, also shows a similar relationship. No periodic precise displacement measurements had been conducted across the ground rupture that cuts through the Magdaong River exposure mapping site (Figures 2a and 8), but the amounts of displacement in the 1990s along this segment (Figure 2) are also far smaller than the scarp heights based on surface profiles across the segments (Figure 5c,d; see Figures 4 and 8 for location of profile). As discussed above, the amounts of creep displacement of the exposed layers of fill and recent sediments at the Magdaong exposure are likewise far smaller than the estimated heights of the pre-existing scarps based on the profiles. This supports the development of creep along pre-existing scarps of tectonic origin.

The Magdaong exposure shows that creep occurs along an active pre-existing tectonic trace and opens the possibility of pre-creep tectonic activity also being associated with the other scarps. Pre-creep tectonic activity along the other creeping segments can also be verified, preferably by less invasive paleoseismic methods.

3.4. Potential for Induced Seismicity

Creep triggered by groundwater withdrawal took advantage of the tectonic structures at the Magdaong River site and, most likely, reactivated the other en echelon structures within the creeping zone. If creep occurs along pre-existing tectonic structures, then the possibility of seismicity triggered by excessive groundwater extraction within the creeping zone should be considered more seriously. The occurrence of induced earthquakes would exacerbate the effects of fault creep that have already been incurred. Excessive groundwater extraction has been known to trigger and alter the timing of earthquakes globally [31–37]. Depressurization due to groundwater withdrawal causes miniscule stress perturbations but are enough to advance the timing of seismicity [33–35,37,38]. It can cause seismicity by triggering stable failure of faults [29,30,39,40] with velocity-strengthening frictional properties [41] through the development of "barriers" and "asperities" [42]. Parameters similar to the criteria listed by Frohlich et al. [43] could be very useful in evaluating whether an earthquake that may occur within and near the creeping zone is induced by groundwater extraction. Succeeding development of bigger barriers and asperities leads to bigger earthquakes [42]. The possibility that sudden fault failure could extend beyond the creeping zone should also be considered. The WVF creeping zone coincides with a dilational jog (Figures 2 and 4) [2,3], which is a feature associated with barriers and asperities [44–47]. These are known sites of rupture initiation and obstacles to slip transfer along faults [48–50]. The 45 km long segment I of the WVF (Figure 1) [2,3] has an estimated return period of 400–600 years and has not moved since 1599 [1]. The failure of the WVF creeping zone due to continued depressurization could induce static stress changes that could advance the failure of segment I or segment III. The weakening of such a barrier could also facilitate contagion during an earthquake originating along either of the adjacent segments. Such contagion is contingent on the ease of the barrier to yield and transfer an additional stress load and on the physical condition of the target segment [51].

4. Conclusions

Most of the active creep scarps occurred along pre-existing scarps with distinct en echelon patterns and strongly correlate with topographic and lithologic boundaries. Large differences between creep displacements and the heights of the pre-existing scarps suggest that the pre-existing scarps have existed long before the earliest suggested occurrence of creep. We have verified the tectonic nature of pre-creep activity through paleoseismic investigation of an exposure of one of the creeping segments.

The tectonic control of the occurrence of creep along the segment exposed in the Magdaong River is indicated by the occurrence of nontectonic creep along a pre-existing surface-rupturing fault zone. The Magdaong site exhibits at least three coseismic events preceding fault creep as interpreted from the upward termination of fault strands in the exposure and the changes in the amount of vertical offset of units with depth. Strike-slip faulting is evident principally from the upward-splaying pattern of the pre-creep fault strands, the relatively small amount of vertical displacement, and the changing unit thickness across the faults. The current creep activity is dominantly vertical, while the pre-creep faulting events are coseismic and dominantly strike-slip. Pre-creep movement along individual segments may not be uniform in terms of the nature of movement (coseismic vs. tectonic creep) and type of faulting. Paleoseismic investigation along the other segments of the creeping zone should provide a better understanding of the individual and collective nature of modern creep and any pre-creep faulting.

Our reservation on the tectonic control along the other segments within the creeping zone is partly due to the lack of pre-existing scarps in some localities as well as the absence of creep along some pre-existing scarps with similar orientation to the creeping faults. Nevertheless, tectonic control is reinforced by the left-stepping en echelon pattern of surface rupturing and distribution along a N-S-trending narrow elongate zone within the dilational gap of the dextral strike-slip WVF. Tectonic control is seemingly not limited to the occurrence of creep along pre-existing structures but is also apparent in the kinematic consistency of individual traces with the active, right-lateral strike-slip faults of the WVF. Vertical displacement is also consistent with compaction due to groundwater withdrawal. Vertical displacement may actually have both tectonic and nontectonic components (e.g., vertical displacement due to compaction). Aside from paleoseismic mapping, future studies may verify tectonic control along the other segments by non-invasive methods, as conducting paleoseismic investigations becomes more difficult in the rapidly developing study area. If the coseismic nature of pre-creep scarps is not recognized and all the displacement along the scarp is attributed to vertical creep due to groundwater extraction, the seismic hazard will be underestimated.

The creep phenomenon in the Sucat–Biñan area has already caused considerable damage to public utilities and residential and commercial buildings. It will continue to do so if groundwater extraction regulations are not strictly enforced in the northern part of the creeping zone and current pumping rates in the south remain unabated. Though stress levels and strengths of the creeping zone and its adjoining segments are yet unknown, the possibility of earthquakes being triggered by continued overextraction of groundwater should be considered by hazard planners.

Author Contributions: Conceptualization, R.E.R. and P.L.K.K.; methodology, R.E.R.; software, R.E.R. and P.L.K.K.; validation, R.E.R. and P.L.K.K.; formal analysis, R.E.R.; investigation, R.E.R.; resources, R.E.R. and P.L.K.K.; data curation, R.E.R.; writing—original draft preparation, R.E.R.; writing—review and editing, P.L.K.K.; visualization, R.E.R.; supervision, P.L.K.K.; project administration, P.L.K.K.; funding acquisition, R.E.R. and P.L.K.K. All authors have read and agreed to the published version of the manuscript.

Funding: This research was funded by the Department of Science and Technology—Philippine Institute of Volcanology and Seismology (DOST-PHIVOLCS) in accordance with the General Appropriations Act of the Republic of the Philippines. A large part of the research was also funded by the research funds of Prof. Knuepfer of the Department of Geological Sciences and Environmental Studies, State University of New York (SUNY) at Binghamton.

Data Availability Statement: The original contributions presented in this study are included in the article. Further inquiries can be directed to the corresponding author.

Acknowledgments: A large part of this work was accomplished with the help of the Department of Science and Technology—Philippine Institute of Volcanology and Seismology (DOST-PHIVOLCS) personnel who provided logistical and moral support. Part of this work was accomplished while at SUNY at Binghamton as a Ph.D. student.

Conflicts of Interest: The authors declare no conflicts of interest.

References

1. Nelson, A.R.; Personius, S.F.; Rimando, R.E.; Punongbayan, R.S.; Tungol, N.; Mirabueno, H.; Rasdas, A. Multiple large earthquakes in the past 1500 years on a fault in metropolitan Manila, the Philippines. *Bull. Seismol. Soc. Am.* **2000**, *90*, 73–85. [CrossRef]
2. Rimando, R.E. Neotectonic and Paleoseismic Study of the Marikina Valley Fault System, Philippines. Ph.D. Dissertation, State University of New York at Binghamton, Binghamton, NY, USA, 2002; 232p.
3. Rimando, R.E.; Knuepfer, P.L. Neotectonics of the Marikina Valley fault system (MVFS) and tectonic framework of structures in northern and central Luzon, Philippines. *Tectonophysics* **2006**, *415*, 17–38. [CrossRef]
4. Rimando, R.E.; Kurita, K.; Kinugasa, Y. Spatial and temporal variation of aseismic creep along the dilational jog of the West Valley Fault, Philippines: Hazard implications. *Front. Earth Sci.* **2022**, *10*, 935161. [CrossRef]
5. Seno, T.; Stein, S.; Gripp, A.E. A model for the motion of the Philippine Sea Plate consistent with NUVEL-l and geological data. *J. Geophys. Res.* **1993**, *98*, 17941–17948. [CrossRef]
6. Philippine Institute of Volcanology and Seismology (PHIVOLCS). Available online: http://faultfinder.phivolcs.dost.gov.ph/ (accessed on 30 July 2024).
7. Ramos, E.G. Subsidence, a serious hazard caused by groundwater extraction in Metro Manila. In Proceedings of the 11th Annual Convention of the Geological Society of the Philippines, Pasig City, Philippines, 2–4 December 1998; pp. 18–30.
8. Raucoules, D.; Le Cozannet, G.; Wöppelmann, G.; Michele, M.; Gravelle, M.; Daag, A.; Marcos, M. High nonlinear urban ground motion in Manila (Philippines) from 1993 to 2010 observed by DInSAR: Implications for sea-level measurement. *Remote Sens. Environ.* **2013**, *139*, 386–397. [CrossRef]
9. Eco, R.C.; Rodolfo, K.S.; Sulapas, J.J.; Morales Rivera, A.M.; Lagmay, A.M.F.; Amelung, F. Disaster in slow motion: Widespread land subsidence in and around Metro Manila, Philippines quantified by Insar time-series analysis. *JSM Environ. Sci. Ecol.* **2020**, *8*, 1068.
10. Burford, R.O.; Harsh, P.W. Slip on the San Andreas fault in central California from alinement array surveys. *Bull. Seismol. Soc. Am.* **1980**, *70*, 1233–1261.
11. Savage, J.C.; Prescott, W.H.; Lisowski, M.; King, N. Geodolite measurements of deformation near Hollister, California, 1971–1978. *J. Geophys. Res.* **1979**, *84*, 7599–7615. [CrossRef]
12. Lienkaemper, J.J.; Borchardt, G.; Lisowski, M. Historic creep rate and potential for seismic slip along the Hayward fault, California. *J. Geophys. Res.* **1991**, *96*, 18261–18283. [CrossRef]
13. Kelson, K.I.; Simpson, G.D.; Lettis, W.R.; Haraden, C.C. Holocene slip rate and earthquake recurrence of the northern Calaveras fault at Leyden Creek, northern California. *J. Geophys. Res.* **1996**, *101*, 5961–5975. [CrossRef]
14. Stenner, H.D.; Ueta, K. Looking for evidence of large surface rupturing events on the rapidly creeping Southern Calaveras fault, California. In Proceedings of the Hokudan International Symposium and School on Active Faulting, Hokudan-cho, Awaji Island, Japan, 13–17 January 2000; pp. 479–486.
15. Yu, S.B.; Liu, C.C. Fault creep on the central segment of the Longitudinal Valley fault, eastern Taiwan. *Proc. Geol. Soc. China* **1989**, *32*, 209–231.
16. Ambraseys, N.N. Some characteristic features of the Anatolian fault zone. *Tectonophysics* **1970**, *9*, 143–165. [CrossRef]
17. Bureau of Mines and Geosciences. *Geology and Mineral Resources of the Philippines*, 1st ed.; Bureau of Mines and Geosciences: Manila, Philippines, 1981; pp. 152–153.
18. Rockwell, T.K. Recognition of individual paleoseismic events in strike-slip environments. In *Directions in Paleoseismology, Proceedings of Conference XXXIX, Albuquerque, NM, USA, 21–23 April 1987*; Crone, A.J., Omdahl, E.M., Eds.; United States Geological Survey: Denver, CO, USA, 1987. Available online: https://pubs.usgs.gov/of/1987/0673/report.pdf (accessed on 16 April 2024).
19. Sieh, K.E.; Williams, P.L. Behavior of the southernmost San Andreas Fault during the past 300 years. *J. Geophys. Res.* **1990**, *95*, 6629–6645. [CrossRef]
20. McCalpin, J.P. Nelson AR Introduction to paleoseismology. In *Paleoseismology*; McCalpin, J.P., Ed.; Academic Press: Orlando, FL, USA, 1996; pp. 1–32.
21. Pavlides, S. First palaeoseismological results from Greece. *Ann. Geofis.* **1996**, *39*, 545–555. [CrossRef]
22. Weldon, R.J.; McCalpin, J.P.; Rockwell, T.K. Paleoseismology of strike-slip tectonic environments. In *Paleoseismology*; McCalpin, J.P., Ed.; Academic Press: Orlando, FL, USA, 1996; pp. 271–329.
23. Ferreli, L.; Michetti, A.M.; Serva, L.; Vittori, E. Stratigraphic evidence of coseismic faulting and aseismic fault creep from exploratory trenches at Mt. Etna Volcano (Sicily, Italy). In *Ancient Seismites*; Ettensohn, F., Rast, N., Brett, C., Eds.; Geological Society of America: Boulder, CO, USA, 2002; pp. 49–62. [CrossRef]
24. Carver, G.A. Geologic criteria for recognition of individual paleoseismic events in compressional tectonic environments. In *Directions in Paleoseismology, Proceedings of Conference XXXIX, Albuquerque, NM, USA, 21–23 April 1987*; Crone, A.J., Omdahl, E.M., Eds.; United States Geological Survey: Denver, CO, USA, 1987.
25. McCalpin, J.P. Geologic criteria for recognition of individual paleoseismic events in extensional environments. In *Directions in Paleoseismology, Proceedings of Conference XXXIX, Albuquerque, NM, USA, 21–23 April 1987*; Crone, A.J., Omdahl, E.M., Eds.; United States Geological Survey: Denver, CO, USA, 1987.

26. Bonilla, M.G.; Lienkaemper, J.J. *Factors Affecting the Recognition of Faults Exposed in Exploratory Trenches*; U.S. Government Printing Office: Washington, DC, USA, 1991; pp. 1–54. [CrossRef]
27. Holzer, T.L. Ground failure induced by ground-water withdrawal from unconsolidated sediment. In *Man-Induced Land Subsidence*; Holzer, T., Ed.; Geological Society of America: Boulder, CO, USA, 1984; Volume 6, pp. 67–105.
28. Hernández-Madrigal, V.M.; Muñiz-Jáuregui, J.A.; Garduño-Monroy, V.H.; Flores-Lázaro, N.; Figueroa-Miranda, S. Depreciation factor equation to evaluate the economic losses from ground failure due to subsidence related to groundwater withdrawal. *Nat. Sci.* **2014**, *6*, 108–113. [CrossRef]
29. Holzer, T.L.; Davis, S.N.; Lofgren, B.E. Faulting caused by groundwater extraction in southcentral Arizona. *J. Geophys. Res.* **1979**, *84*, 603–612. [CrossRef]
30. Segall, P. Earthquakes triggered by fluid extraction. *Geology* **1989**, *17*, 942–946. [CrossRef]
31. Gonzalez, P.J.; Tiampo, K.F.; Palano, M.; Cannavo, F.; Fernandez, J. The 2011 Lorca earthquake slip distribution controlled by groundwater crustal unloading. *Nat. Geosci.* **2012**, *5*, 821–825. [CrossRef]
32. Amos, C.B.; Audet, P.; Hammond, W.C.; Bürgmann, R.; Johanson, I.A.; Blewitt, G. Uplift and seismicity driven by groundwater depletion in central California. *Nature* **2014**, *509*, 483–486. [CrossRef]
33. Kundu, B.; Vissa, N.K.; Gahalaut, V.K. Influence of anthropogenic groundwater unloading in Indo-Gangetic plains on the 25 April 2015 Mw 7.8 Gorkha, Nepal earthquake. *Geophys. Res. Lett.* **2015**, *42*, 10607–10613. [CrossRef]
34. Kundu, B.; Vissa, N.K.; Gahalaut, K.; Gahalaut, V.K.; Panda, D.; Malik, K. Influence of anthropogenic groundwater pumping on the 2017 November 12 M7.3 Iran-Iraq border earthquake. *Geophys. J. Int.* **2019**, *218*, 833–839. [CrossRef]
35. Foulger, G.R.; Wilson, M.P.; Gluyas, J.G.; Julian, B.R.; Davies, R.J. Global review of human-induced earthquakes. *Earth Sci. Rev.* **2018**, *178*, 438–514. [CrossRef]
36. Wu, W. A review of unloading-induced fault instability. *Undergr. Space* **2021**, *6*, 528–538. [CrossRef]
37. Ellsworth, W.L. Injection-induced earthquakes. *Science* **2013**, *341*, 142–147. [CrossRef]
38. Tiwari, D.K.; Jha, B.; Kundu, B.; Gahalaut, V.K.; Vissa, N.K. Groundwater extraction-induced seismicity around Delhi region, India. *Sci. Rep.* **2021**, *11*, 10097. [CrossRef]
39. Segall, P. Stress and subsidence resulting from subsurface fluid withdrawal in the epicentral region of the 1983 Coalinga earthquake. *J. Geophys. Res.* **1985**, *90*, 6801–6816. [CrossRef]
40. Segall, P. Induced stresses due to fluid extraction from axisymmetric reservoirs. *Pure Appl. Geophys.* **1992**, *139*, 535–560. [CrossRef]
41. Guglielmi, Y.; Cappa, F.; Avouac, J.P.; Henry, P.; Elsworth, D. Seismicity triggered by fluid injection-induced aseismic slip. *Science* **2015**, *348*, 1224–1226. [CrossRef]
42. Pennington, W.D.; Davis, S.D.; Carlson, S.M.; Dupree, J.; Ewing, T.E. The evolution of seismic barriers and asperities caused by the depressuring of fault planes in oil and gas fields of South Texas. *Bull. Seismol. Soc. Am.* **1986**, *76*, 939–948.
43. Frohlich, C.; DeShon, H.; Stump, B.; Hayward, C.; Hornbach, M.; Walter, J.I. A historical review of induced earthquakes in Texas. *Seismol. Res. Lett.* **2016**, *87*, 1022–1038. [CrossRef]
44. Scholz, C.; Engelder, J.T. The role of asperity indentation and ploughing in rock friction. I. Asperity creep and stick slip. *Int. J. Rock Mech. Min. Sci.* **1976**, *13*, 149–154. [CrossRef]
45. Aki, K. Characterization of barriers on an earthquake fault. *J. Geophys. Res.* **1979**, *84*, 6140–6148. [CrossRef]
46. Lay, T.; Kanamori, H.; Ruff, L. The asperity model and the nature of large subduction zone earthquakes. *Earthq. Predict. Res.* **1982**, *1*, 3–71.
47. Sibson, R.N. Effects of fault heterogeneity on rupture propagation. In *Directions in Paleoseismology, Proceedings of Conference XXXIX, Albuquerque, NM, USA, 21–23 April 1987*; Crone, A., Omdahl, E., Eds.; United States Geological Survey: Denver, CO, USA, 1987.
48. Bakun, W.H.; Stewart, R.M.; Bufe, C.G.; Marks, S.M. Implication of seismicity for failure of a section of the San Andreas fault. *Bull. Seismol. Soc. Am.* **1980**, *70*, 185–201. [CrossRef]
49. King, G.; Nábělek, J. Role of fault bends in the initiation and termination of earthquake rupture. *Science* **1985**, *228*, 984–987. [CrossRef]
50. King, G.C.P. Speculations on the geometry of the initiation and termination processes of earthquake rupture and its relation to morphology and geological structure. *Pure Appl. Geophys.* **1986**, *124*, 567–585. [CrossRef]
51. Perkins, D.M. Contagious fault rupture, probabilistic hazard, and contagion observability. In *Directions in Paleoseismology, Proceedings of Conference XXXIX, Albuquerque, NM, USA, 21–23 April 1987*; Crone, A.J., Omdahl, E.M., Eds.; United States Geological Survey: Denver, CO, USA, 1987; pp. 428–439. Available online: https://pubs.usgs.gov/of/1987/0673/report.pdf (accessed on 20 April 2024).